Hydrol. Earth Syst. Sci. Discuss., 3, 1215–1248, 2006
www.hydrol-earth-syst-sci-discuss.net/3/1215/2006/

Hydrology and Earth System Sciences Discussions

Papers published in *Hydrology and Earth System Sciences Discussions* are under open-access review for the journal *Hydrology and Earth System Sciences*

Novel evaporation experiment to determine soil hydraulic properties

K. Schneider[1], **O. Ippisch**[2], **and K. Roth**[1]

[1]Institute of Environmental Physics, University of Heidelberg, Heidelberg, Germany
[2]Interdisciplinary Center for Scientific Computing, University of Heidelberg, Heidelberg, Germany

Received: 24 April 2006 – Accepted: 27 April 2006 – Published: 29 June 2006

Correspondence to: K. Schneider (klaus.schneider@iup.uni-heidelberg.de)

Abstract

A novel experimental approach to determine soil hydraulic material properties for the dry and very dry range is presented. Evaporation from the surface of a soil column is controlled by a constant flux of preconditioned air and the resulting vapour flux is measured by infrared absorption spectroscopy. The data are inverted under the assumptions that (i) the simultaneous movement of water in the liquid and vapour is represented by Richards' equation with an effective hydraulic conductivity and that (ii) the coupling between the soil and the well-mixed atmosphere can be modelled by a boundary layer with a constant transfer resistance. The optimised model fits the data exceptionally well. Remaining deviations during the initial phase of an experiment are thought to be well-understood and are attributed to the onset of the heat flow through the column which compensates the latent heat of evaporation.

1 Introduction

Movement of soil water is usually described by Richards' equation (Jury et al., 1991). A crucial part of this are the hydraulic material properties, in particular the soil water characteristic $\theta_\ell(\psi_m)$ and the hydraulic conductivity function $K(\theta_\ell)$. However, these properties are difficult to measure directly (Topp and Miller, 1966) which led to the development of inverse methods. Most popular today is multi-step outflow (Eching et al., 1994; van Dam et al., 1994) which evolved from one-step outflow (Parker et al., 1985). In these methods, gas pressure p_g in the soil sample equals ambient atmospheric pressure, as is the case in soils, while the pressure p_ℓ in the liquid phase at the lower end of the sample is reduced in one or more steps. Correspondingly, the matric potential $\psi_m = p_\ell - p_g$ in the sample is reduced and the resulting flow of water is recorded. Obviously, these methods are fundamentally limited to $\psi_m > -100\,\mathrm{kPa}$ since p_ℓ must be larger than the vapour pressure of water. Practical limitations like the permeability of the phase separator at the lower boundary are more strict and typically lead to

$\psi_m > -20$ kPa. The method is thus only applicable for the range of moderately negative potentials, hence to the rather wet range of soils. This is no real limitation for many processes which primarily operate in this range, including groundwater recharge and solute transport through soils to groundwater. Other processes, however, cannot be described reliably with material properties estimated from such a limited potential range. The reason for this is that the corresponding parameterisations are empirical relations with no physical foundation. Hence, extrapolation is not possible without strong assumptions on the porous media. Notorious examples where representations for the dry range are required include plant water uptake, soil-atmosphere coupling, and optimal dry-land farming.

A further practical difficulty with multi-step outflow experiments concerns the rapid change of the boundary condition which may lead to a violation of the assumption of local quasi-static equilibrium states that is inherent in the Richards formulation. This can be expected to be particularly severe in coarse-textured media, for which the experimental method is inherently well suited.

A seemingly simple way to circumvent the fundamental limitation of multi-step outflow measurements would be to keep p_ℓ constant at ambient atmospheric pressure and to increase p_g. Since there is no fundamental limit to increasing p_g, ψ_m can be made arbitrarily negative. However, the water phase now is in a state completely different from that in a natural soil with the same value of ψ_m. This is easily appreciated by considering a tensiometer in the two situations. Since the relation between the water contents of these two states is unknown, the parameters are not transferable.

The limitations of multi-step outflow experiments for estimating hydraulic material properties can be overcome by evaporation experiments, as they allow virtually unlimited values of the matric potential (by making the air above the surface dry). Gardner and Miklich (1962) were the first to propose such experiments. Their setup was basically retained in later studies (Wendroth et al., 1993; Tamari et al., 1993). A typical experimental setup is shown in Fig. 1. The soil is initially saturated, and then free evaporation is allowed to start. At times t_i, the potentials $\psi_{m_{ij}}$ at heights z_j are measured

with tensiometers and the cumulative outflow is monitored using a balance. Additionally, at the end of the experiment the total residual water is measured gravimetrically, thus obtaining the real water content θ_i for each measurement time t_i. There arise a number of fundamental difficulties with this approach, however: (i) The most severe issue are the tensiometers required for measuring the matric potential. This again sets a lower limit for the applicable matric potential. While the exact value of this limit depends on the location of the uppermost tensiometer – Šimůnek et al. (1998) showed in numerical studies that measuring the potential closer to the surface improves the results – as well as on the soil hydraulic properties, it is typically on the order of -100 kPa for water tensiometers. If the potential falls below the air-entry value of the tensiometer or below the vapour pressure of water, whichever is higher, then water is released from the tensiometer into the soil. This leads to a disturbance of the measurements that may be quite dramatic. (ii) A severe technical challenge results from the very small potential gradients in regions where the hydraulic conductivity is still high. Here, the accuracy of the tensiometers becomes limiting. As a consequence, the method becomes inaccurate near saturation. (iii) Finally, weighing for determining the water flux becomes increasingly difficult as the flux decreases. Dangling cables and air movement, e.g. due to air conditioning, or dust become significant sources of uncertainty and demand special precautions.

To overcome these drawbacks, we retain the basic idea of an evaporation experiment but take a new experimental approach that gets rid of the balance and of the tensiometers. The basic idea is to force evaporation with a well-controlled potential in the head space above the soil column and to accurately measure the resulting vapour flow. The data are then inverted for the coefficients of some parameterisation of the soil hydraulic properties with an accurate model that also accounts for the coupling between soil and head space. We chose the Mualem-Brooks-Corey parameterisation for the material properties and assumed a surface boundary layer with a constant transfer resistance.

2 Theory

We model the soil column as a uniform one-dimensional medium and assume that its soil water characteristic may be described by the Brooks-Corey parameterisation

$$\Theta_\ell(\psi_m) = \frac{\theta_\ell(\psi_m) - \theta_r}{\theta_s - \theta_r} = \begin{cases} [\psi_m/\psi_e]^{-\lambda} & ;\psi_m < \psi_e \,, \\ 1 & ;\psi_m \geq \psi_e \,, \end{cases} \tag{1}$$

and its hydraulic conductivity function by the corresponding Mualem parameterisation

$$K(\Theta_\ell) = K_s \Theta_\ell^{\tau+2+2/\lambda} \,. \tag{2}$$

To model vapour transport through the soil colum, we assume local thermodynamic equilibrium. Then, the molar water vapour content v_g^w is given by (Rawlins and Campbell, 1986)

$$v_g^w = \frac{p_s^w(T)}{RT} \exp\left(\frac{\psi_m V_m^w}{RT}\right) , \tag{3}$$

where V_m^w is the molar volume of liquid water, and $p_s^w(T)$ the partial pressure of water vapour over pure liquid water at temperature T. It can be described with Magnus' formula (Murray, 1967) as

$$p_s^w(T) = 610.78\,\text{Pa}\ \exp\left(\frac{17.2694(T - 273.16\,\text{K})}{T - 35.86\text{K}}\right) . \tag{4}$$

These relations can also be used to calculate the equivalent matric potential from a given water vapour concentration.

The equivalent flux $\boldsymbol{j}_g^w$ of liquid water transported by diffusion of water vapour is given by

$$\boldsymbol{j}_g^w = -V_m^w D_g^w \nabla v_g^w , \tag{5}$$

which we can reformulate, using the chain rule, as

$$\boldsymbol{j}_g^w = -V_m^w D_g^w \left(\frac{\partial v_g^w}{\partial T}\nabla T + \frac{\partial v_g^w}{\partial \psi_m}\nabla\psi_m\right) . \tag{6}$$

If we neglect the temperature dependent part, approximate the vapour by an ideal gas, and use Eq. (3) we get:

$$\boldsymbol{j}_g^w = -D_g^w \frac{p_s^w(T) {V_m^w}^2 \exp\left[\frac{\psi_m V_m^w}{RT}\right]}{[RT]^2} \nabla\psi_m \tag{7}$$

To account for tortuosity ξ, the model

$$\xi(\theta_\ell) = \frac{\theta_\ell^2}{\theta_s^{2/3}} , \tag{8}$$

was used (Jin and Jury, 1996). The diffusion of water vapour is not hindered as much by liquid films as that of other gases, because it can condensate on one side and re-evaporate on the other. While Philip and de Vries (1957) limit this effect to thermal induced vapour flow, it appears plausible that it also holds for isothermal vapour transport. Therefore the saturated water content θ_s was used for θ_ℓ in the tortuosity model yielding the relation $D_g^w = \theta_s^{4/3} D_{g,\text{atm}}^w$, where $D_{g,\text{atm}}^w$ is the diffusion coefficient for water vapour in free air. We finally obtain

$$\boldsymbol{j}_g^w = -D_{g,\text{atm}}^w \frac{\theta_s^{4/3} p_s^w(T) {V_m^w}^2 \exp\left(\frac{\psi_m V_m^w}{RT}\right)}{[RT]^2} \nabla\psi_m \tag{9}$$

which has the same form as the Buckingham-Darcy flux

$$\boldsymbol{j}_\ell^w = -K_\ell(\theta_\ell)\nabla\psi_m \,. \tag{10}$$

Hence, Richards' equation may be enhanced to include vapour transport in the soil column by writing

$$\frac{\partial \theta_\ell}{\partial t} = \nabla \cdot \left[[K_\ell(\theta_\ell) + K_g(\psi_m)] \nabla \left[\psi_m - \rho_\ell^w g z \right] \right] \tag{11}$$

with

$$K_g(\psi_m) = D_{g,\mathrm{atm}}^w \frac{\theta_s^{4/3} p_s^w(T) {V_m^w}^2 \exp\left(\frac{\psi_m V_m^w}{RT}\right)}{[RT]^2} \,. \tag{12}$$

A crucial step is the representation of the upper boundary. We model it as a diffusive layer of constant thickness r_b and assume that the time scale of diffusion across this layer is much smaller than the time scale on which the boundary condition changes. This appears reasonable since the time scale of diffusion, given by $r_b^2/[2D_{g,\mathrm{atm}}^w]$, is some 0.1 s for a layer thickness of 2 mm. The vapour flux across such a layer is given by

$$j_{\mathrm{boundary}}^w = -\frac{V_m^w D_{g,\mathrm{atm}}^w}{RT} \frac{p_{\mathrm{exp}}^w - p_s^w(T) \exp\left(\frac{\psi_m V_m^w}{RT}\right)}{r_b} \tag{13}$$

where p_{exp}^w is the partial pressure of water vapour in the well-mixed head space above the soil column. We comment that, by definition, the processes in this layer are not resolved well. In particular its physical location is not defined, i.e., the fraction of the layer that is within the soil column, and the porosity of the respective parts of the soil. However, for the type of thin layer we consider here all these complicating factors only enter as a constant of proportionality. Hence, we make r_b a fitting parameter that absorbs all these factors. Obviously, its value then cannot be interpreted physically anymore.

3 Experimental setup

The soil sample is contained in a PVC cylinder of 81 mm radius and 100 mm height. The bottom of the column is closed. The top of the soil column is closed by a 30 mm high gas-tight head space (evaporation chamber, Fig. 2). A constant flow of air is established through the head space to remove the water vapour and thereby set the potential. Filters prevent dirt from entering the measurement system. The difference of water vapour content before and after the evaporation chamber and the air flow through the chamber quantify the water flux at the upper boundary of the soil sample, while the relative humidity and the temperature in the evaporation chamber define the equivalent matric potential of the air.

An infrared absorption gas analyser simultaneously measures the water vapour molar fraction x (mole/mole) before and after the soil sample. Temperature T is measured at the air inlet of the chamber, the total pressure p in the chamber. Inside the chamber the air is mixed with a fan to ensure uniform water vapour content and thus a well-defined potential. The gas flow q is measured by the pressure jump across a capillary with known conductivity. It is controlled by a vacuum pump with adjustable speed. A time domain reflectometry (TDR) sensor (Robinson et al., 2003) is installed vertically in the soil column to measure the total water content. The individual parts of the setup are described in the following.

3.1 Air conditioning

To enable a well-defined boundary condition, the air is conditioned before it enters the evaporation chamber, i.e. its water vapour content is set to a defined value. This is done with a cold trap. The air flows through an aluminium box with flow channels. The box is cooled by Peltier elements. Abundant water freezes out in the box, thus the outgoing air has defined water vapour content. The current through the Peltier elements is regulated based on the temperature of the gas at the outlet of the box by a controller. After the box the air is passively warmed to ambient temperature.

As time passes, more and more water freezes out at the walls. Therefore, there are two identical coolers. If one box becomes frozen up, the incoming air stream is switched to the other box by magnetic valves, and the first box is defrosted, so it is ready again to use when the second one is frozen up.

3.2 Infrared gas analyser

The Licor LI-7000 infrared gas analyser (LI-COR Inc., 2004) used for measuring water vapour content uses the 2595 nm absorption band. The instrument has a thermal light source and uses an optical bandpass filter to select the appropriate wavelength. No spectral information is needed. Two cells A and B independently measure water vapour molar fraction.

Calibration measurements are required for zero point, span and zero absorption value. The calibration procedure is to let known gases flow through the cells of the instrument, wait for the measurements to stabilise and then execute the corresponding user calibration functions.

Calibration gas is generated with a dew point generator: Air is bubbled through a water bath whose temperature is precisely controlled by a series of peltier thermoelectric coolers. The accuracy of water vapour content of the generated air stream is ±0.2°C between 0°C and 50 °C, drift is specified as less than 0.02°C. Additionally, water free null gas (here, N_2 4.6, H_2O<5 ppm (volume)) is used for zero point calibration.

To test the accuracy of the gas analyser, the dew point generator was set to 10°C and the conditioned air was then flown through both cells, resulting in a zero molar fraction difference. Results are shown in Fig. 3. Noise is very low (about 0.01 mmol/mol in cell B measurement and 0.005 mmol/mol in molar fraction difference). In accordance with the statement of the manufacturer, the molar fraction difference is much more stable than the absolute value. Cell B drift is about 0.05 (mmol/mol)/h, molar fraction difference drift about 0.002 (mmol/mol)/h. Thus the instrument is very precise. Drift can be kept low by regular calibration.

To check the calibration and the linearity of the instrument, water-free null gas was

used as reference gas flowing through cell A and calibration gas with a defined dew point, generated with the dew point generator, was flowing through cell B. Several dew point values were set and the corresponding measured water vapour molar fractions p_{meas} were recorded. Previously, all zero and span calibrations had been made. The partial pressures corresponding to the nominal dew point values were calculated using Magnus' formula, Eq. (4). As can be seen in Fig. 4, the instrument is quite linear through the measured range and the deviation from the nominal molar fraction is small.

3.3 Runtime calibration

Since a typical evaporation experiment can last for several weeks, the gas analyser must be calibrated during runtime. This is done by switching the measurement gas stream using bistable magnetic valves, such that it flows through a bypass. Then, calibration gas is flown through both cells of the gas analyser, and when values become stable, the calibration routines are executed. No measurements can be taken during that time. After calibration completed, it is switched back to normal operation. The setup is sketched in Fig. 5.

It is generally desirable to keep the evaporation conditions during calibration as steady as possible, to ensure that the data can validly be interpolated during that time. While calibration is running, the conductivity of the system the measurement gas goes through increases: the bypass has a higher conductivity than the measurement cells (including the air filters). To keep the flow rate through the system constant, the pump rate is lowered during calibration. Accordingly, the pressure in the evaporation chamber changes. This does not matter however, as the evaporation process is not sensitive to pressure changes.

When switching back, a small amount of residual calibration gas enters the evaporation chamber. This has virtually no effect on the evaporation process, because the volume of the measurement cells is neglectable compared to the incoming air stream: $\tau = V_{\mathrm{cell}}/q \approx 11\,\mathrm{cm}^3/500\,\mathrm{l/h} \approx 2.3\,\mathrm{min} \ll \tau_{\mathrm{dynamics}}$.

3.4 Gas flow measurement

The gas flow through the system is measured by the pressure drop on a capillary. With laminar flow, the relation between the gas flow q and the pressure difference Δp is linear. As the flow will not be totally laminar, a second order polynomial was used. The coefficients a_i were determined by a calibration measurement: The flow q was measured with a rotameter, several flow rates were set and the corresponding $(\Delta p, q)$ data pairs were recorded. Then the polynomial was fitted through the data.

3.5 Data filtering

As mentioned in Sect. 3.3, the pressure in the measurement system changes during runtime calibration. These pressure peaks need some time to decay after switching back to normal mode. As explained above, the pressure jumps do not disturb physical information. However they bother data continuity, because the gas analyser is sensitive to pressure jumps. Therefore, the pressure peaks are filtered out (Fig. 6): for each calibration process, a line is fitted through the last 20 data points before the calibration had started using linear regression. The first point after the time when the calibration process finished whose value is within twice the standard deviation of the line is defined as end point. The time difference between the end point and the end of the calibration process is limited to 10 min. All points between the start of the calibration and the end point are discarded.

3.6 Water flux at the upper boundary

The water flux is calculated from the total air flow through the system q and the difference of the molar fraction of water vapour $x_d = x_B - x_A$. For the flow in units of mole,

$$\dot{v}_g^w = x_d \dot{v}_g \tag{14}$$

where $\dot{v}_g^w$ denotes water vapour flow and $\dot{v}_g$ total gas flow, both in units of mole. It is assumed that the water vapour molar fraction is constant during one measurement,

because the measurement is very fast compared to the time scale of soil dynamics. Employing the ideal gas law, the final relation

$$j_{\mathrm{exp}}^w = \frac{V_m^w}{RA} \frac{x_d p q}{T} \tag{15}$$

for the water flux at the upper boundary j_{exp}^w is obtained, where p is the total pressure in the evaporation chamber and A the area of the soil surface.

4 Inverse modelling

Hydraulic parameters were estimated from the measurements using inverse modelling. We used a numerical forward model together with the Levenberg-Marquardt algorithm. The forward model integrated Richards' equation using a cell-centred finite-volume scheme with full-up-winding in space and an implicit Euler scheme in time. Linearisation of the nonlinear equations is done by an inexact Newton method with line search. The linear equations are solved with a direct solver. For the time solver the time step is adapted automatically. A no-flux condition was used for the lower boundary. At the upper boundary the evaporation was calculated by Eq. (13). To account for the temperature dependence of the equivalent conductivity of the vapour phase the measured temperature at the upper boundary was always used for the whole soil. The sensitivities required by the Levenberg-Marquardt algorithm were derived by external numerical differentiation.

5 Results

Two test measurements were made, one with a sand sample and one with an undisturbed sample from a sandy loam soil (Grenzhof sample).

5.1 Sand sample

Sand with grain size below 0.25 mm (density ρ_s=2.65 g/cm^3) was filled in the PVC sample cylinder. The sand was filled into water, such that the water level was always above the sand, to prevent entrapped air. The evaporation chamber including the vertical TDR sensor was installed at the top of the sample.

An MSO experiment was run as a standard experiment to bring the sample into a semi-dry state. The lower boundary condition was first set to 0 kPa for 2 h and then changed in 0.5 kPa steps from −2 kPa to −8 kPa, each step lasting 3 h (0.1 kPa correspond to 1 cm water column). The last step was continued until 69.4 h, where the MSO was terminated. The water was removed from the base at the lower boundary and the evaporation experiment was started. At t=236.9 h, the experiment was terminated.

Figure 7 shows the outflow at the lower boundary during MSO and the flux density at the upper boundary during evaporation, respectively. The shape of the evaporation flux is as one would expect, with a rapid decay to a zero flux: The conductivity decreases rapidly as the sample dries out.

The peaks at t=113 h were caused by an aberration in cold trap temperature: for 10 min, the temperature deviated by maximal +2.3°C from its nominal value. This resulted in a higher H_2O concentration in the incoming air stream, hence a higher potential (Fig. 8). This jump in potential caused a smaller evaporation rate, which is seen in the flux, Fig. 7. This demonstrates the high sensitivity of the experimental setup.

The total water content was measured by TDR (Fig. 9). The increase upon switching from MSO to evaporation is caused by water in the ceramic plate which is required in the MSO setup. This plate is 13 mm thick and has the same diameter as the soil sample. Its porosity is 0.34 with air entry value of about −1.2 kPa. The plate was not removed after MSO because this would have disturbed the soil sample, generating uncontrollable modifications. It was just disconnected from the rest of the system. Therefore the 4.4 mm water contained in the ceramic plate entered the soil sample

during evaporation.

Total water content change is about 0.39, 0.057 of it during evaporation. This corresponds to a total outflow of 39 mm (5.7 mm during evaporation). Integrating the flux during the evaporation period results in a total cumulative outflow of 8.9 mm. The total outflow (MSO and evaporation) is 43.8 mm. The difference is explained quite well by the 4.4 mm water which entered the sample from the ceramic plate. The remaining difference is attributed to a disturbance of pore geometry by the TDR probe. When the sensor is inserted into the sand, the soil matrix is modified such that round the rods larger pores are created. Thus, the pore size distribution surrounding the TDR probe is slightly changed to larger pores. When the potential becomes more negative, these larger pores are drained first, thus the TDR sensor detects a smaller water content which is not representative for the whole sample. This effect is also demonstrated by MSO: The water content measured by TDR shows large outflow at smaller potentials than actually recorded at the lower boundary (compare Figs. 7 and 9).

Figure 10 shows the relative error of the evaporation measurements. The error of the gas analyser measurement was estimated from the test measurements (Sect. 3.2). The error of the gas flow measurement was estimated using the noise of the pressure transducer and the error of the coefficients of the polynomial, which was determined by the fit program. The latter include the error of rotameter and pressure readings during calibration, as these errors were given as weights to the fit function. The accuracy of the temperature and pressure measurement was ±0.2 K and ±0.05 kPa, respectively. All errors were calculated using Gaussian error propagation.

The water flux error is about 4.5% to 5%, the error of the boundary condition about 1% to 2%. The major part of the error of the water flux results from the gas flow measurement using the capillary. Thus, the accuracy can be improved easily by using a more precise gas flow measurement device.

5.2 Undisturbed soil sample

With MSO as the first experiment, one has to address hysteresis. During MSO, water is sucked out at the lower boundary. Then the direction of water flow is reverted and water evaporates from the upper boundary. This is generally difficult to model since hysteresis is not yet understood sufficing well. Thus, MSO was abandoned and evaporation was started directly. After 640 h, the experiment was terminated.

The measured flux and potential is shown in Fig. 11. Integrating the flux resulted in a cumulative outflow of (27.1±1.3) mm. Weighing the sample before and after the experiment yielded (26.5±0.5) mm. The aberration in the boundary condition around t=300 h was caused by heating of the laboratory. Its result on evaporation can be seen in the flux rate, emphasising the correctness of the data.

Figure 12 shows the total water content, measured by TDR. The permittivity of the soil matrix was determined based on volumetric porosity and water content measurements as well as TDR bulk permittivity measurements on the field site when the sample was taken during an excavation. The total change in water content is (25±3) mm. This is consistent with the flux and weight measurements. The Figure also shows the mass balance $\eta\theta_l(t) + \int_0^t j^w_{\exp}(\tau)d\tau$, where η denotes the height of the sample. It is assumed to be constant during the whole measurement. The decrease at the beginning is again attributed to larger pores around the TDR rods which were created by the insertion of the probe, analogous to the sand sample. Because these larger pores are drained first, the measured water content was not representative for the whole sample. As the potential became more negative, the smaller pores in the undisturbed part of the sample were drained as well and the real water content again matched the one measured by TDR.

The relative error is shown in Fig. 13. Again, the potential error is 1% to 2% and water flux error 4.5% to 5%. This high data quality is crucial for the quality of the result of the inversion process.

Hydraulic parameters were estimated from the measured values using the inverse

model described in Sect. 4. Only evaporation rates were used as target variables. Fitted parameters are the Brooks-Corey parameters λ and ψ_e, the saturated hydraulic conductivity K_s, the available water content $\theta_s - \theta_r$, and the effective thickness r_b of the boundary layer. The value of τ was fixed at 0.5 as suggested by Mualem (1976). A grid convergence study gave a necessary spatial resolution of 0.125 mm equivalent to 880 grid points.

Figure 11 illustrates that for times t>30 h, the optimised model response is in excellent agreement with the data. For shorter times, however, the model is obviously not capable to describe the data. We think that this results from thermal processes that are not represented in the model. At the start of the experiment, the entire column is in thermal equilibrium. With the onset of evaporation, latent heat is consumed right at the saturated soil surface. As a consequence, the temperature drops there and with it the vapour pressure of water. Hence, with Eq. (13), the evaporation flux will be reduced. In its current formulation, our model does not include the effect of latent heat and therefore yields a gross over-prediction of the evaporation flux. As a consequence, the data for t<30 h were not used for the inversion.

For longer times, both the drying front and the temperature front penetrate deeper into the soil with the consequence that evaporation occurs over a larger interval and that temperature depressions are much smaller. This leads to the eventual excellent agreement between model and data. In particular we notice that the aberration caused by the heating of the laboratory is easily reproduced by the model. While such an agreement is no prove that the model is correct, it is a strong hint that it may be used as an effective representation of the real system under similar conditions as those encountered during the experiment. The resulting parameters are given in Table 1. While we do not have any independent confirmation, they appear reasonable for the soil under examination.

6 Conclusions

We presented a novel experimental approach to evaporation experiments for determining soil hydraulic properties. A detailed error analysis demonstrated the very high accuracy of the new technique which is further confirmed by the rapid and consistent response of the measured flux to small fluctuations of the boundary condition.

The high data quality and the correct representation of the underlying physics are crucial for the quality of the numerical inversion. The excellent agreement between measured and simulated data for longer times are a strong indication that all the relevant processes, within our window of view, are captured by the Richards' equation with an effective hydraulic conductivity function that explicitly incorporates vapour transport and with a constant effective diffusive boundary layer at the soil-atmosphere interface. For shorter times, the discrepancy between data and model require the inclusion of additional processes. Qualitatively, the deviations can be understood in terms of latent heat consumed by the evaporating water. In the current model formulation, this process and the associated transport of heat is not included.

The main advantage of our new approach over traditional evaporation experiments is that it yields data right from the soil surface to which the inversion is most sensitive. Practical advantages include (i) a large and uniform measurement range that is achieved by directly measuring the flux and by the boundary condition which can be controlled in a wide range through the air flow and air conditioning and (ii) a constant and rather high accuracy for arbitrarily sized soil samples. In addition, the method is applicable directly in the field after minor modifications and it is an excellent tool for detailed studies of evaporation from porous media. With all the advantages, a final caveat is in order. The cost of the instrumentation is rather high when commercial equipment is used.

Appendix A

List of symbols

Superscripts w and a denote water and air, respectively. Subscripts g and ℓ denote the gas phase and the liquid phase, respectively.

j	volumetric flux (m/s)
p_g	pressure in gas phase (Pa)
p_ℓ	pressure in liquid phase (Pa)
p	total pressure (Pa)
p_s^w	saturation partial pressure of water vapour over pure water (Pa)
q	air flow (m^3/s)
t	time (s)
x	molar fraction (mol/mol)
z	height (m)
D	diffusion coefficient (m^2/s)
$D_{g,\mathrm{atm}}^w$	diffusion coefficient for water vapour in air ($2.1\times10^{-5}\,m^2s^{-1}$)
K	hydraulic conductivity ($m^2\,Pa^{-1}\,s^{-1}$)
R	universal gas constant ($8.3145\,J\,mol^{-1}\,K^{-1}$)
T	temperature (K)
V_m^w	molar volume of liquid water ($1.804\times10^{-5}\,m^3\,mol^{-1}$)
η	sample height (m)
λ	Brooks-Corey parameter (–)
ν	molar density (mol/m^3)
ψ_m	matric potential (J/m^3=Pa)
ψ_e	air entry value (J/m^3=Pa)
ρ_ℓ^w	density of liquid water ($998\,kg/m^3$)
θ	volumetric water content (m^3/m^3)
θ_s	saturated volumetric water content (m^3/m^3)
θ_r	residual volumetric water content (m^3/m^3)
ξ	tortuosity coefficient (–)

References

Eching, S. O., Hopmans, J. W., and Wendroth, O.: Unsaturated hydraulic conductivity from transient multistep outflow and soil water pressure data, Soil Sci. Soc. Am. J., 58, 687–695, 1994. 1216

Gardner, W. R. and Miklich, F. J.: Unsaturated conductivity and diffusity measurements by a constant flux method, Soil Sci. Soc. Am. J., 93, 271–274, 1962. 1217

Jin, Y. and Jury, W. A.: Characterizing the Dependence of Gas Diffusion Coefficient on Soil Properties, Soil Sci. Soc. Am. J., 60, 66–71, 1996. 1220

Jury, W. A., Gardner, W. R., and Gardner, W. H.: Soil Physics, John Wiley & Sons, New York, 5th edn., 1991. 1216

Mualem, Y.: A new model for predicting the hydraulic conductivity of unsaturated porous media, Water Resour. Res., 12, 513–522, 1976. 1230

Murray, F. W.: On the Computation of Saturation Vapor Pressure, J. Appl. Meteorol., 6, 203–204, 1967. 1219

Parker, J. C., Kool, J. B., and van Genuchten, M. T.: Determinig soil hydraulic properties from one-step outflow experiments by parameter estimation: II. Experimental studies, Soil Sci. Soc. Am. J., 49, 1354–1359, 1985. 1216

Philip, J. R. and de Vries, D. A.: Moisture Movement in Porous Materials under Temperature Gradients, Trans. Am. Geophys. Union (EOS), 38, 222–232, 1957. 1220

Rawlins, S. L. and Campbell, G. S.: Water potential: Thermocouple Psychrometry, in: Methods of Soil Analysis, Part 1. Physical and Mineralogical Methods, edited by: Klute, A., Agronomy Series 9, 597–618, American Society of Agronomy, Madison, WI, 2nd edn., 1986. 1219

Robinson, D. A., Jones, S. B., Wraith, J. M., Or, D., and Friedman, S. P.: A review of advances in dielectric and electrical conductivity measurement in soils using time domain reflectometry, Vadose Zone J., 2, 444–475, 2003. 1222

Šimůnek, J., Wendroth, O., and van Genuchten, M. T.: Parameter Estimation Analysis of the Evaporation Method for Determining Soil Hydraulic Properties, Soil Sci. Soc. Am. J., 62, 894–905, 1998. 1218

Tamari, S., Bruckler, L., Halbertsma, J., and Chadoeuf, J.: A Simple Method for Determining Soil Hydraulic Properties in the Laboratory, Soil Sci. Soc. Am. J., 57, 642–651, 1993. 1217

Topp, G. C. and Miller, E. E.: Hysteretic moisture characteristics and hydraulic conductivities for glass-bead media, Soil Sci. Soc. Am. Proc., 30, 156–162, 1966. 1216

van Dam, J. C., Stricker, J. N. M., and Droogers, P.: Inverse method to determine soil hydraulic functions from multistep outflow experiments, Soil Sci. Soc. Am. J., 58, 647–652, 1994. 1216

Wendroth, O., Ehlers, W., Hopmans, J. W., Kage, H., Halbertsma, J., and Wösten, J. H. M.: Reevaluation of the Evaporation Method for Determining Hydraulic Functions in Unsaturated Soils, Soil Sci. Soc. Am. J., 57, 1436–1443, 1993. 1217

Table 1. Resulting parameters for the Grenzhof soil.

parameter	fitted value
λ(–)	1.03±0.1
ψ_e (Pa)	1020±40
K_s (cm/h)	0.116±0.009
$\theta_s - \theta_r$ (m^3/m^3)	0.306±0.002
r_b (mm)	2.74±0.05

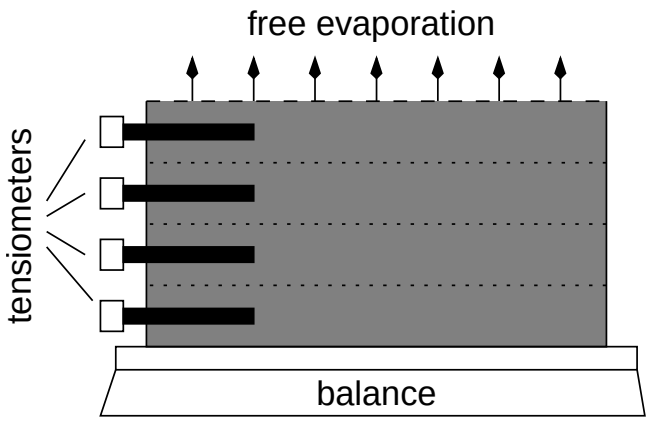

Fig. 1. Schematic of the standard setup of evaporation experiments.

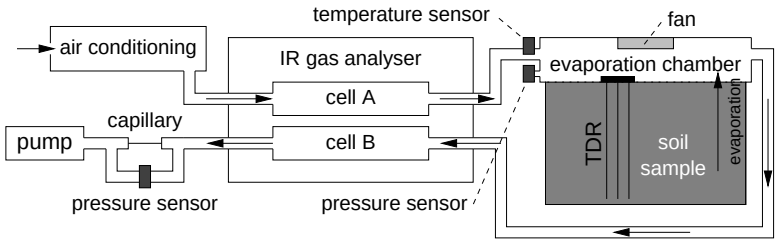

Fig. 2. Experimental setup. Evaporation takes place into a gas-tight head space (evaporation chamber) above the soil surface. Air is flowing through it to take away the water. Water vapour molar fraction is measured before and after the head space. The air is conditioned before it enters the chamber to set a well defined boundary condition. The gas flow is measured with a capillary and controlled with a vacuum pump with adjustable speed.

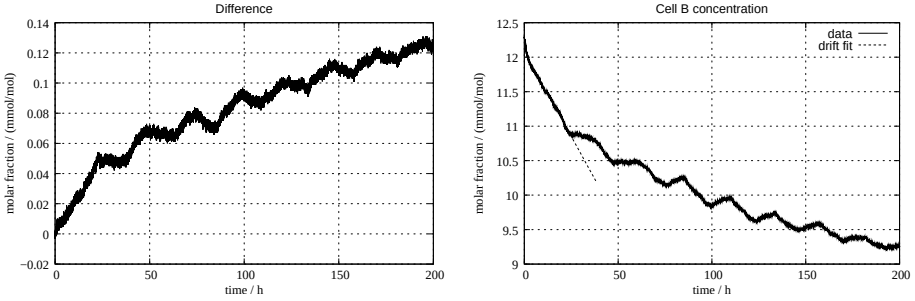

Fig. 3. Water vapour molar fraction measurements of the gas analyser with conditioned air at 10°C dew point flowing simultaneously through both cells of the instrument. The difference (left) is very stable while the absolute molar fraction (right) is drifting faster, with about $-49\,\mu$mol mol^{-1} h^{-1} on the first day (dashed line).

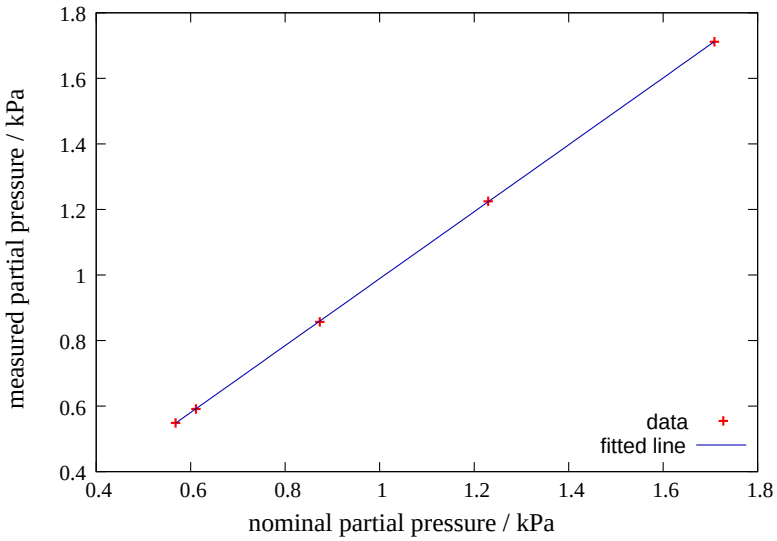

Fig. 4. Linearity and calibration check of the gas analyser. Null gas was flowing through cell A and air with defined water vapour molar fraction through cell B. The nominal cell B molar fraction was varied and the measured partial pressure p_{meas} recorded.

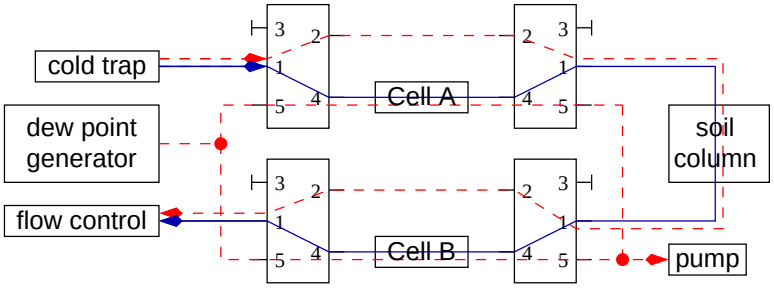

Fig. 5. Setup for runtime calibration. In normal operation (blue line), all valves are in state (1). During calibration (red dashed lines), the four valves are set to state (2), the measured gas bypasses the gas analyser and conditioned air from the dew point generator is flowing through both cells.

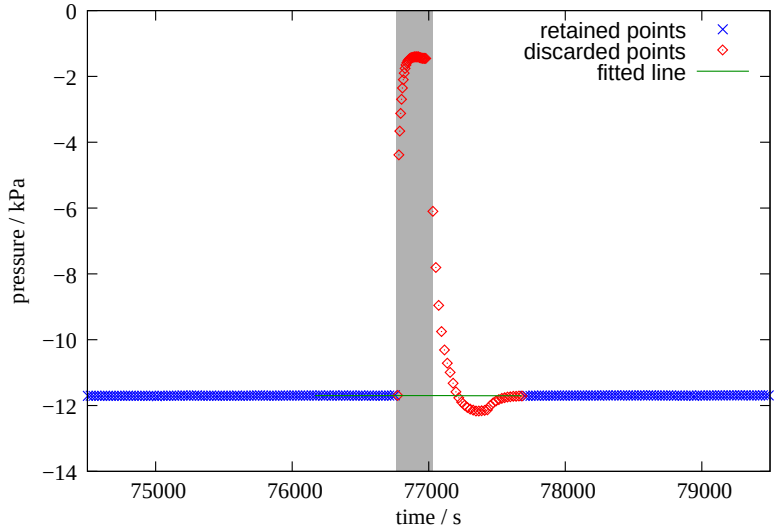

Fig. 6. Filtered data of the pressure in the evaporation chamber. The data is displayed as points, the ones which were discarded in red and the ones retained in blue. The fitted line is displayed in green, the time of the actual calibration process is marked as a gray band.

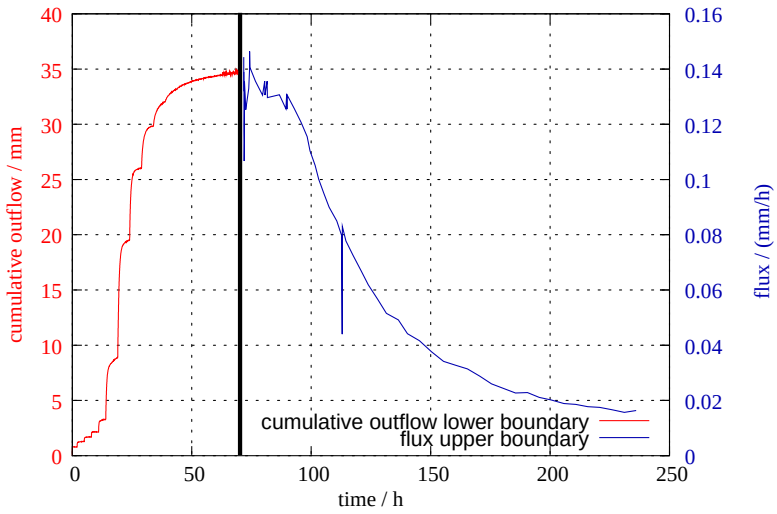

Fig. 7. Measured outflow of the sand sample. The red line shows the cumulative outflow at the lower boundary during MSO, the blue line the flux rate at the upper boundary during the evaporation experiment. The black vertical line marks the switch between MSO and evaporation.

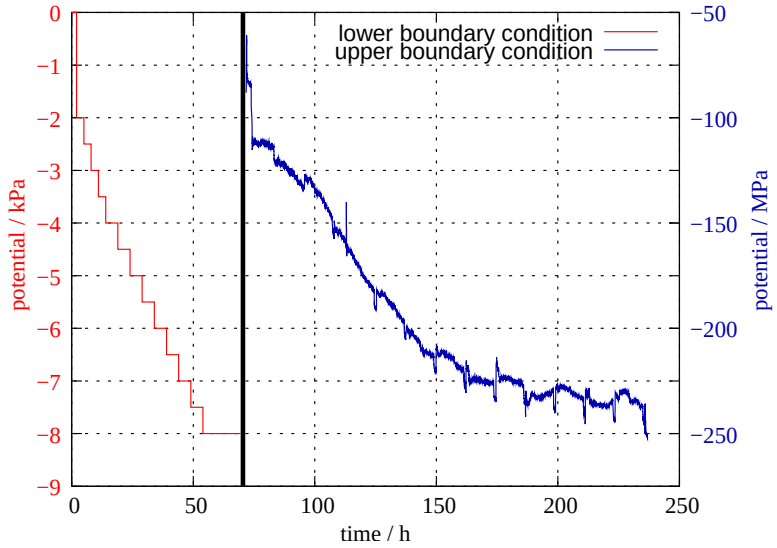

Fig. 8. Boundary conditions during the experiment with the sand sample. The red line shows the lower boundary condition during the MSO, the blue line the upper boundary condition during the evaporation experiment. A no-flow boundary condition was set at the upper boundary during MSO and at the lower boundary during evaporation. The black vertical line marks the switch between MSO and evaporation.

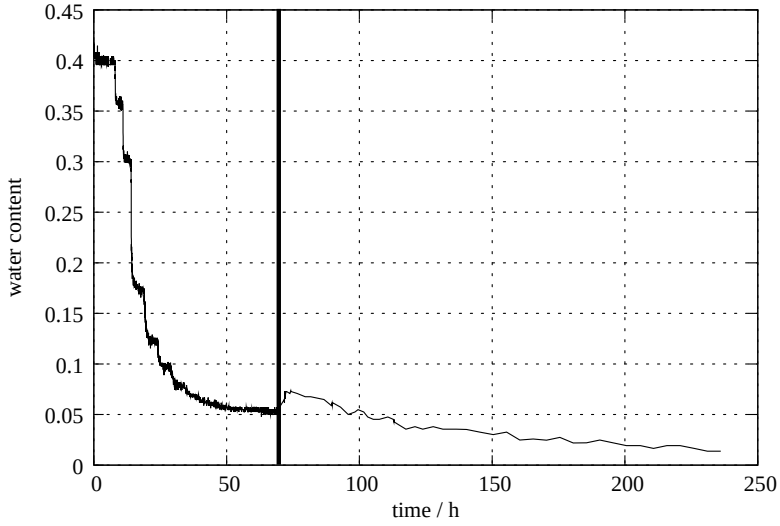

Fig. 9. Total water content of the sand sample, measured by TDR. The black vertical line marks the switch between MSO and evaporation.

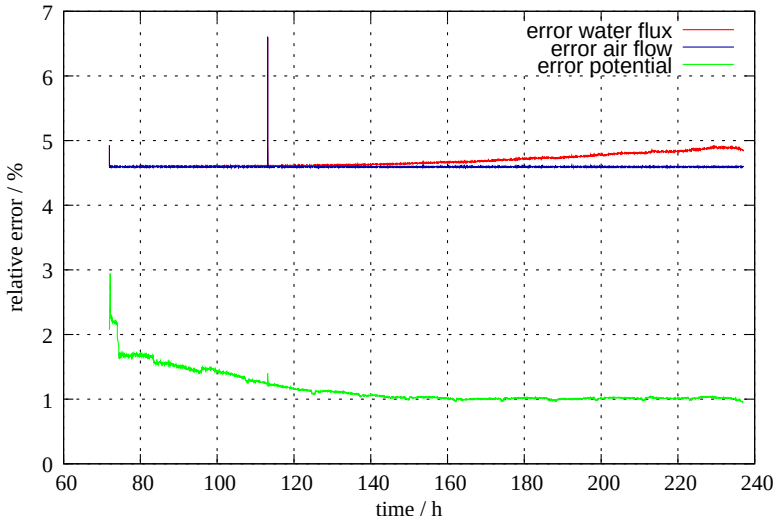

Fig. 10. Relative error of the evaporation measurements of the sand sample.

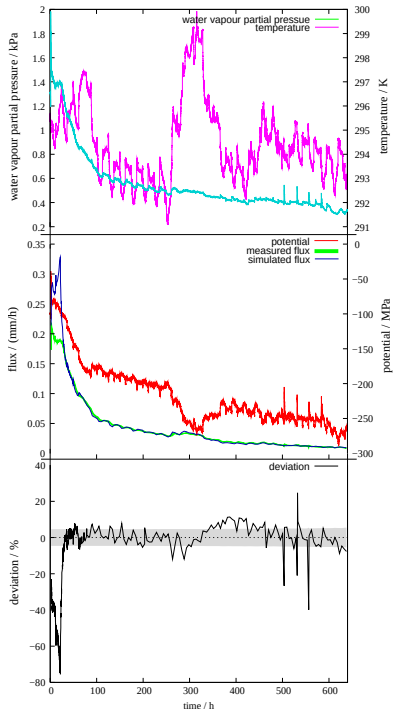

Fig. 11. Results of the evaporation experiment with the Grenzhof soil sample. Notice that measured and simulated flux (middle frame) practically overlap. The relative deviation $(j^w_{\mathrm{exp}} - j^w_{\mathrm{model}})/j^w_{\mathrm{exp}}$ is shown in the bottom frame together with the measuring uncertainty from Fig. 13 (gray band).

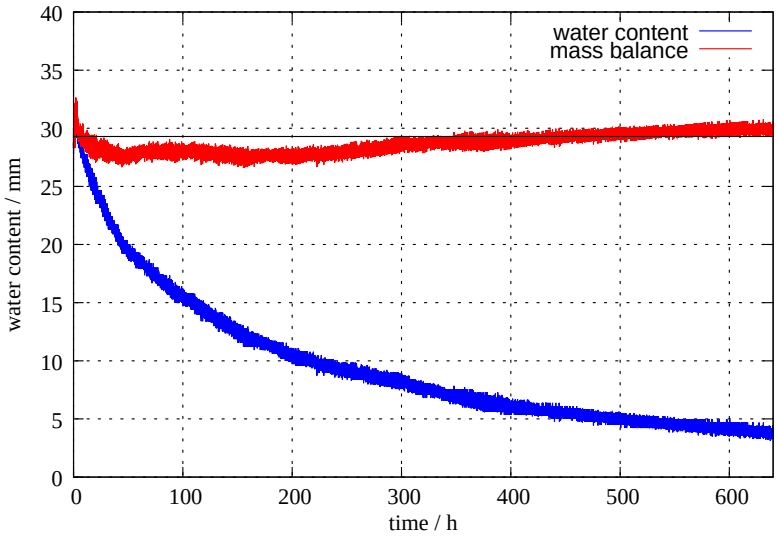

Fig. 12. Total water content of the Grenzhof soil sample, measured by TDR (blue), and the mass balance $\eta\theta_l(t) + \int_0^t j^w_{\text{exp}}(\tau)d\tau$ (red). The black horizontal line represents the initially measured water content.

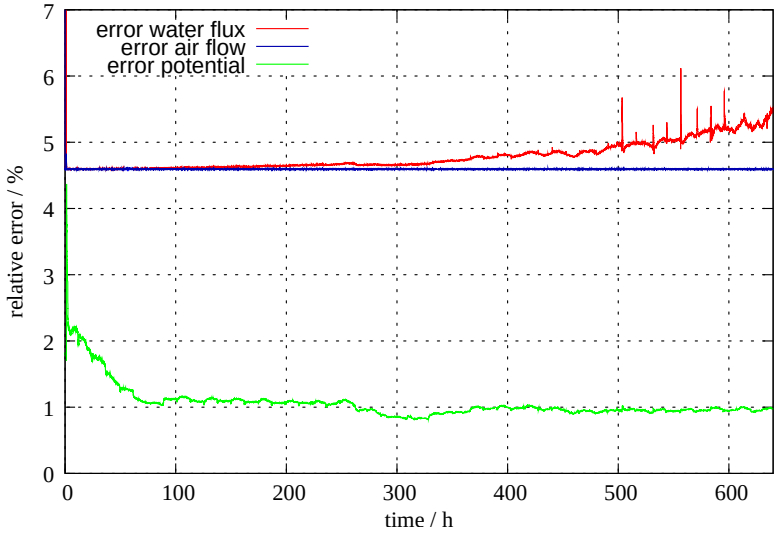

Fig. 13. Relative error (1σ) of the evaporation measurement of the Grenzhof soil sample.